J Neurophysiol 123: 1870–1885, 2020.
First published March 11, 2020; doi:10.1152/jn.00536.2019.

RESEARCH ARTICLE | *Modularity and Compositionality in Motor Control: Acknowledging Emilio Bizzi*

Separating neural influences from peripheral mechanics: the speed-curvature relation in mechanically constrained actions

James Hermus,[1] Joseph Doeringer,[2] Dagmar Sternad,[3] and Neville Hogan[1,4]

[1]*Department of Mechanical Engineering, Massachusetts Institute of Technology, Cambridge, Massachusetts;* [2]*Department of Engineering, HighRes Biosolutions, Beverly, Massachusetts;* [3]*Departments of Biology, Electrical and Computer Engineering and Physics, Northeastern University, Boston, Massachusetts; and* [4]*Department of Brain and Cognitive Sciences, Massachusetts Institute of Technology, Cambridge, Massachusetts*

Submitted 19 August 2019; accepted in final form 1 March 2020

Hermus J, Doeringer J, Sternad D, Hogan N. Separating neural influences from peripheral mechanics: the speed-curvature relation in mechanically constrained actions. *J Neurophysiol* 123: 1870–1885, 2020. First published March 11, 2020; doi:10.1152/jn.00536.2019.—While the study of unconstrained movements has revealed important features of neural control, generalizing those insights to more sophisticated object manipulation is challenging. Humans excel at physical interaction with objects, even when those objects introduce complex dynamics and kinematic constraints. This study examined humans turning a horizontal planar crank (radius 10.29 cm) at their preferred and three instructed speeds (with visual feedback), both in clockwise and counterclockwise directions. To explore the role of neuromechanical dynamics, the instructed speeds covered a wide range: fast (near the limits of performance), medium (near preferred speed), and very slow (rendering dynamic effects negligible). Because kinematically constrained movements involve significant physical interaction, disentangling neural control from the influences of biomechanics presents a challenge. To address it, we modeled the interactive dynamics to "subtract off" peripheral biomechanics from observed force and kinematic data, thereby estimating aspects of underlying neural action that may be expressed in terms of motion. We demonstrate the value of this method: remarkably, an approximately elliptical path emerged, and speed minima coincided with curvature maxima, similar to what is seen in unconstrained movements, even though the hand moved at nearly constant speed along a constant-curvature path. These findings suggest that the neural controller takes advantage of peripheral biomechanics to simplify physical interaction. As a result, patterns seen in unconstrained movements persist even when physical interaction prevents their expression in hand kinematics. The reemergence of a speed-curvature relation indicates that it is due, at least in part, to neural processes that emphasize smoothness and predictability.

NEW & NOTEWORTHY Physically interacting with kinematic constraints is commonplace in everyday actions. We report a study of humans turning a crank, a circular constraint that imposes constant hand path curvature and hence should suppress variations of hand speed due to the power-law speed-curvature relation widely reported for unconstrained motions. Remarkably, we found that, when peripheral biomechanical factors are removed, a speed-curvature relation reemerges, indicating that it is, at least in part, of neural origin.

Address for reprint requests and other correspondence: J. Hermus, Department of Mechanical Engineering, MIT, 77 Massachusetts Ave, 3-143, Cambridge, MA 02139 (e-mail: jhermus@mit.edu).

constrained motion; mechanical impedance; predictability; rhythmic movements; two-thirds power law

INTRODUCTION

Experimental studies of motor neuroscience should start with macroscopic behavior, as there are some remarkably robust patterns that can guide the investigation of neural control of movement (Krakauer et al. 2017). One such pattern robustly observed in curved motions is a relation between hand path curvature and speed: hand speed decreases as curvature increases. This finding has been widely reported in unconstrained movements for more than 30 years, although its implications for neural control have been controversial (Abend et al. 1982; Catavitello et al. 2016; Dayan et al. 2007; Gribble and Ostry 1996; Hicheur et al. 2005; Huh and Sejnowski 2015; Lacquaniti et al. 1983; Massey et al. 1992; Schaal and Sternad 2001; Schwartz 1994; Viviani and Flash 1995; Viviani and Stucchi 1989; Viviani and Terzuolo 1982; Zago et al. 2018). Specifically, the discussion debated whether this robust relation is due to biomechanical or neural influences. To further examine how biomechanical factors may influence or give rise to this robust speed-curvature relation, the present study examined a simple constrained-motion task to test whether this pattern persists even when mechanical conditions prevent its expression. It did, suggesting that the speed-curvature relation is present in the neural organization of action.

While human dexterity vastly exceeds that of modern robots, the human neuromechanical system is orders of magnitude slower than its robotic counterparts (Kandel et al. 2013; Loram et al. 2005; Shepard and Metzler 1971). Slow neural transmission and muscle response implies that humans have to rely heavily on feed-forward (i.e., predictive) control, especially when physically interacting with objects and environments where bidirectional interaction forces arise. Prior work on the control of dynamically complex objects showed that humans adjust their behavior to prioritize predictability of the object dynamics (Bazzi et al. 2018; Maurice et al. 2018a; Nasseroleslami et al. 2014; Sternad 2017; Sternad and Hasson 2016).

Here we extend the study of predictability to kinematically constrained actions.

One way to move predictably is to move smoothly, as rapid rates of change, i.e., nonsmooth jerky movements, compromise the ability to predict future states. Smoothness, quantified by minimal mean-squared jerk, has been demonstrated in numerous studies of unconstrained reaching (Flash and Hogan 1985; Hogan 1982, 1984; Nelson 1983; Sternad et al. 2010). Interestingly, smoothness can also account for the relation between hand path curvature and tangential speed. For simple curves (e.g., ellipses), this is the so-called "two-thirds power law," as hand speed decreases at regions with higher curvature in a robust power law (Lacquaniti et al. 1983; Richardson and Flash 2002; Schaal and Sternad 2001; Sternad and Schaal 1999; Viviani and Flash 1995). More complex curves display more complex relations, a "spectrum of power laws" (Huh and Sejnowski 2015). Importantly, in all cases, a temporal coincidence between extrema of tangential speed and path curvature is derived from theory and observed in practice. A power-law speed-curvature relation is consistent with a preference for smoothness and predictability.

Much of the previous neuroscience literature has focused on simple unconstrained movements, typically reaching and pointing. While these paradigms have rendered manageable data for analysis and modeling, it is difficult to generalize the insights gained to understand tasks that involve physical interaction, essential in any kind of tool use. While some animals are capable of making and using tools, this ability is vastly more developed in humans (Boesch and Boesch 1990; Hunt 1996; Johnson-Frey 2004; Kenward et al. 2005). Physical interaction is a significant challenge in robotics (Colgate and Hogan 1989, 1988; Paul 1987; Whitney 1977). It is, therefore, quite remarkable that, despite the feedback delays in the motor system, humans maintain stability in everyday tasks. Many tools and daily interactions with the environment introduce kinematic constraints, such as turning a steering wheel, opening a door, and turning a crank. For example, opening a door or turning a steering wheel confines the hand to a planar circular path with constant curvature; if the speed-curvature relation generalizes to object manipulation, no speed fluctuations should be evoked. However, if that relation is of primarily neural origin, it may still influence behavior, even in this situation. This study tested whether a speed-curvature relation—a corollary of predictability—was present in the neural command, even in those cases.

A central challenge in motor neuroscience is to tease apart the contributions of neural control and biomechanics, a problem that is even more pronounced during interactive tasks. During physical interaction, a limb is fundamentally subject to at least two sets of inputs for every output: force exerted on an object depends not only on neural activity, but also on the object's motion. The relation between displacement and the force it evokes may be characterized mathematically by mechanical impedance (a dynamic generalization of stiffness). In principle, knowledge of mechanical impedance combined with simultaneous measurement of force and motion during object manipulation would allow us to "subtract off" or "peel back" peripheral biomechanics to uncover underlying neural influences. In practice, mechanical impedance is nonlinear and time-varying, and measuring it during movement, although possible, is challenging (Bennett et al. 1992; Guarín and Kearney 2017; Lacquaniti et al. 1993; Lee et al. 2016; Lee and Hogan 2015; Rouse et al. 2013, 2014; van de Ruit et al. 2020). Moreover, measurement inevitably introduces perturbations that may alter behavior.

An alternative (pursued here) is to approximate mechanical impedance using a plausible mathematical model based on measurements made under static postural conditions. Given this model and observations of actual motion and exerted force, we define a construct that we call the "zero-force trajectory," the trajectory that would have been followed if the external forces were zero. The zero-force trajectory summarizes one consequence of neural activity and expresses it as a quantity that may be compared with actual motion. To evaluate its sensitivity to the uncertainty about mechanical impedance, the results were tested over a wide range of parameter variations.

Motion under a circular constraint, i.e., turning a crank, imposes a constant curvature hand path. If a speed-curvature relation applies to hand motion during object manipulation, turning a crank should not elicit any variation of hand speed. However, the zero-force trajectory is not confined to the constant curvature of the circle. If a speed-curvature relation, consistent with smoothness and predictability, is a feature of neural control, it should be manifest in the consequence of neural action that is expressed by the zero-force trajectory. The central hypothesis tested in this study was that a systematic relation between curvature and speed would reemerge in observations of the zero-force trajectory.

To create a rich data set to afford subtracting off the influences of inertial mechanics and neuromuscular dynamics, crank-turning was studied at preferred speed, and three speeds covering a wide range: *1*) a speed close to the fastest that subjects could manage, such that inertial effects predominate; *2*) a speed near subjects' preferred or comfortable speed; and *3*) an extremely slow speed, such that the action was quasi-static and all dynamic effects were negligible. To encourage movements with constant speed along the constant curvature path, we provided a visual display of instructed speed, together with visual feedback of actual hand speed. As inertial behavior is strongly directional and varies with limb position, we examined clockwise and counterclockwise rotation.

Remarkably, we found that, when peripheral biomechanics were subtracted, independent of the direction of rotation, the zero-force trajectory exhibited a coincidence of curvature and speed extrema resembling that reported for unconstrained motion.

METHODS

Participants

Ten healthy male college-aged students were recruited for the study. All participants were right-handed, and none reported any biomechanical injury to their arm nor any neurological problems. All participants gave informed, written consent before the experiment. The informed consent and experimental protocol were reviewed and approved by the Institutional Review Board for the Massachusetts Institute of Technology.

Experimental Apparatus and Procedure

The crank used in this experiment is shown in Fig. 1. The crank arm was mounted on a high-precision incremental optical encoder/

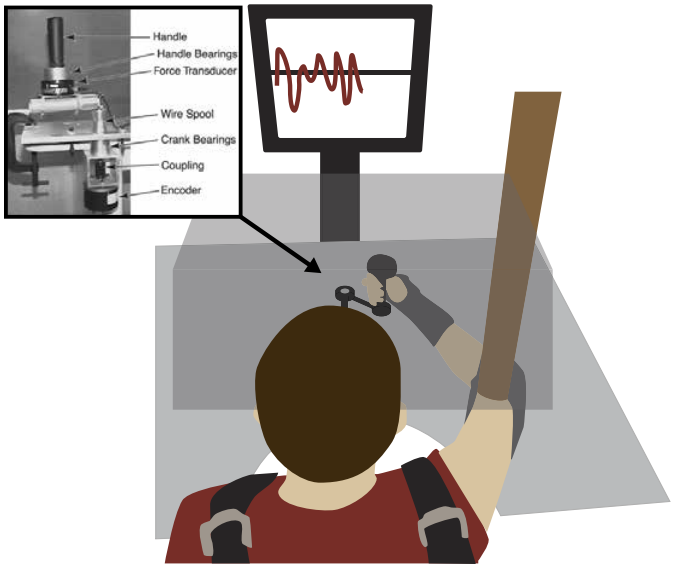

Fig. 1. Experimental setup. The crank displayed in the *inset* was used to provide a circular constraint. Vision of the arm and crank was occluded, but the subject was provided with visual speed feedback. The wrist was braced, the elbow was supported by a sling, and the shoulders were strapped to a chair.

interpolator set (Gurley Precision Instruments encoder no. 8335-11250-CBQA, interpolator no. HR2-80QA-BRD) with a resolution of 0.0004 degrees per count. A six-axis force transducer (ATI model 15/50) was attached to the end of the crank, with a handle mounted on it. A spool managed the force transducer cable.

During the experiment, the subject's arm was occluded from view by a wooden structure, which did not limit the range of motion. The arm was suspended by a canvas sling connected to the ceiling; the arm and forearm were in the plane of the crank. The subject sat in a chair with a rigid back, while the shoulder was constrained by a harness attached to the back of the chair. The subject was positioned such that the crank, with radius of 10.29 cm, was well within the work space of the arm.

Data acquisition was controlled by a computer running the QNX real-time operating system on an Intel Pentium 100 processor. The encoder, sampling at 200 Hz, was connected to a set of counters and to the computer via digital I/O. The ATI force transducer's signal, sampled at 100 Hz, was processed by its embedded controller and input to the computer through the digital I/O. The visual display, also generated by the computer, was on a 17-in. monitor (311 × 238 mm, resolution 1,280 × 1,024, 76 Hz), which was mounted ~75 cm from the subjects' eyes. The experiment was divided into two unequal sections: two blocks of trials at subjects' preferred or comfortable speed, and six blocks of trials at a visually instructed speed. The design of the experimental conditions is graphically overviewed in Fig. 2.

At the start of the experiment, subjects performed 20 trials at their preferred speed, 10 trials in clockwise (CW) direction and 10 in counterclockwise (CCW) direction. Both conditions were blocked, in random sequence for each subject, and each trial lasted 8 s. Subjects were not provided any visual feedback during these trials. Thereafter, subjects performed 6 blocks of 30 trials, each with visual specification of 1 of 3 target speeds [slow: 0.075, medium: 0.5, and fast: 2.0 revolutions per second (rev/s)], in either CW or CCW directions (Fig. 2). The order of the speed and direction blocks was pseudorandomized across subjects. The three speeds were selected to cover a significant range: 0.075 rev/s was extremely slow (required over 13 s per revolution), 0.5 rev/s was close to subjects' preferred speed, and 2.0 rev/s was close to the fastest speed at which subjects could turn the crank. Visual feedback on the monitor displayed the target speed, as well as subjects' real-time hand speed: the horizontal axis was time, and the vertical axis was speed. Subjects' speed was estimated using an online backward finite difference algorithm. Target speed was displayed as a continuous horizontal line in the middle of the screen. The relation between crank motion and screen display was rescaled for every block; the width of the screen corresponded to the time of the trial, which was a function of the desired crank speed. Seven trials in each block were "blind" catch trials, in which visual feedback of the actual hand speed was removed, while the display of target speed was retained. For each speed direction block, one distribution of catch trials was chosen and kept the same for all subjects. The placing of catch trials was different for each block. The pseudorandomizing of catch trials ensured that there was at least one trial with visual feedback before each catch trial.

In the slow-speed conditions, each trial lasted 45 s; in the medium-speed conditions, each trial lasted 16 s; and in the fast-speed conditions, each trial lasted 4 s. This yielded 8 turns of the crank for the fast and medium conditions, but only ~3.4 turns of the crank for the slow condition. The duration of the slow-speed trials was chosen as a compromise between acquiring adequate data and avoiding subject fatigue.

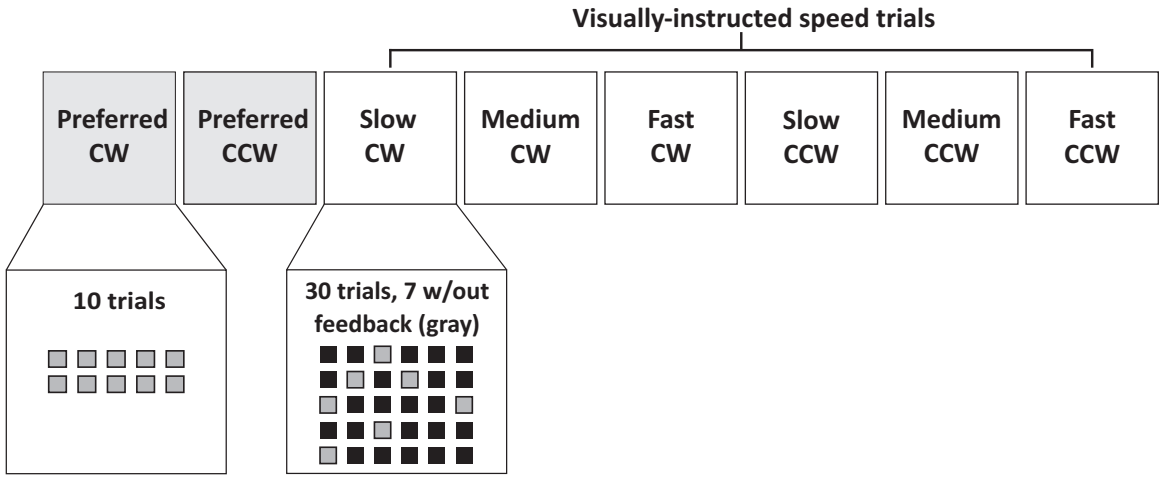

Fig. 2. Experimental design. Each of the 10 subjects completed 20 trials at their preferred speed without visual feedback: 10 trials in clockwise (CW) and 10 trials in counterclockwise (CCW) directions. In the instructed-speed trials, subjects completed 30 trials in each condition. Visual feedback was not provided for 7 of the 30 trials during each of the instructed-speed blocks.

Data Processing and Analysis

Crank speed and normal force were computed with respect to crank angle divided into 360 angle bins. As the different target speeds were sampled at the same rate for different trial durations, they contained a different number of samples per bin. Therefore, the data were interpolated to the largest number of samples, which was 9,001 samples at the slowest target speed, 0.075 rev/s. The interpolation was performed using a piece-wise cubic Hermite interpolating polynomial (Fritsch and Carlson 1980). After interpolation, the speed or force profiles were binned into 360 sections corresponding to a full rotation of the crank. Then the mean of the samples in each bin was taken, resulting in a speed or force profile over 360 crank angles. In all trials, the first 1.5 s were discarded to eliminate transients before calculating summary measures. Dependent measures were mean speed, standard deviation (SD) of speed, mean normal force, and SD of normal force.

Trials at preferred speed. To characterize subjects' preferred behavior, we tested whether the mean normal force was significantly different from zero, and whether turning direction influenced the dependent measures. The speed mean and standard deviation (SD) were computed for the initial 10 trials performed at the preferred speed. Then these quantities were averaged to produce a mean speed and SD for each subject. Mean force and SD of force were similarly averaged for each subject. One subject moved much faster than all others (beyond 2 SDs of the other subjects). His data were excluded from subsequent analysis of the preferred speed trials.

Student's *t* tests were used to detect whether the mean normal force was significantly different from zero. Paired-sample *t* tests were carried out to test for significant effects of turning direction on mean speed and normal force. Significance values of post hoc *t* tests were adjusted using the Šídák–Bonferroni procedure, where the original significance level was defined as $\alpha = 0.05$, the number of *t* tests was m, and the corrected Šídák–Bonferroni significance values were: $\alpha_{SID} = 1 - (1 - \alpha)^{1/m}$. All statistical analyses were performed using the SPSS statistical software package (SPSS Inc., Chicago, IL). Before these analyses, a Shapiro–Wilk test was performed on each of the dependent measures to determine whether these data were drawn from a normal distribution. In most cases, the assumption was met at a 5% significance level. However, in four cases, the Shapiro–Wilk test detected a violation. In three of the four cases, a single outlier was the cause; the remaining case had two outliers. In each case, when the outlier was removed, the Shapiro–Wilk test no longer detected a violation of the normality assumption. Furthermore, the inclusion or exclusion of these outliers did not change the statistical significance of the tests. Thus only parametric tests were used in this analysis.

Trials at instructed speeds. In the first trial of the blocks in which speed and direction were instructed, subjects often did not achieve the task goal: they occasionally turned in the wrong direction, did not complete a full cycle, or turned at the wrong speed. Hence, the first trial in each block was discarded. The seven "catch" trials, without visual feedback, were omitted from initial statistical analysis. The speed mean and SD were computed for each of the remaining trials.

To quantify the influence of speed and direction, a linear mixed model was employed; it was then tested using analysis of variance (ANOVA). The linear model, which represented the observed dependent measure $Y_{i,j,k}$ was expressed as

$$Y_{i,j,k} = \mu_T + \alpha_j + \beta_k + \gamma_l(\alpha\beta)_{j,k} + (\alpha\gamma)_{j,l} + (\beta\gamma)_{k,l} + (\alpha\beta\gamma)_{j,k,l} + E_{i,(j,k,l)} \quad (1)$$

where the grand mean is μ_T, the fixed effect of speed is α_j, where j is an index from 1 to 3, the fixed effect of direction is β_k, were k is an index from 1 to 2, the random effect of subject is γ_l, where l is an index from 1 to 10, and the stochastic sampling effect is $E_{i,j,k}$, where i is an index from 1 to 22 (representing the number of trials excluding the first and the 7 catch trials). As above, all statistical analyses were performed using the SPSS statistical software package (SPSS Inc., Chicago, IL); the significance level was set to 5%.

Simulation of passive inertial mechanics. Physical interaction with a kinematic constraint changes the nonlinear inertial mechanics with which the neuromuscular system interacts. Despite the familiarity of this constrained-motion task, a failure to compensate perfectly for these changes might account for some of the observed patterns of force and motion. To provide insight about these nonlinear and nonintuitive effects, we simulated the fluctuations of speed and force that would be predicted from the configuration-dependent variation of inertial mechanics subject to this kinematic constraint; the simulations excluded any contribution from muscle action. The arm was modeled as a two-link planar serial linkage, with no gravitational or frictional effects. Inertial parameters were estimated based on the cadaver studies of Dempster (Miller and Nelson 1973; Plagenhoef 1971). The shoulder joint was located at the thorax, which was assumed to be stationary. This approach is the same as that used by Ohta et al. (2004). The dynamics of the arm coupled to the crank are detailed in APPENDIX A. The variation of motion due to closed-chain inertial dynamics was simulated. In these model simulations, all joint torques, generated by muscle and by friction, were set to zero. The system was initialized at the 3 o'clock position, with initial angular velocities set to the three target speeds: slow, medium, and fast. Numerical integration was performed using MATLAB's ode45 algorithm (Shampine and Reichelt 1997).

Zero-Force Trajectories

To describe the dynamics of interaction, a mechanical impedance operator was used: $Z\{\cdot\}$ (Hogan 1985a, 1985b). The force time-function $F(t)$ was computed from the displacement time-function $\Delta x(t)$, $F(t) = Z\{\Delta x(t)\}$. Displacement was defined as $\Delta x(t) = x_0(t) - x(t)$, where $x(t)$ was the actual hand position and $x_0(t)$ was a zero-force trajectory. Although muscle force production is a complex function of many factors, its dominant behavior could be well-described by a function of muscle length and its rate of change (Hill 1938; Joyce et al. 1969; Rack and Westbury 1969). Accordingly, a simplified model of muscle mechanical impedance was used: a linear spring and viscous damping element with common displacement (Hogan 1984). To implement this model on a two-joint arm, joint stiffness was assumed to be a 2×2 symmetric matrix, independent of configuration. Joint damping, also a 2×2 symmetric matrix, was proportional to joint stiffness. This was similar to the muscle model previously used by Flash (1987), although the damping term was defined relative to the zero-force trajectory.

The joint torque was defined by

$$\tau = \boldsymbol{K}(\boldsymbol{q}_0 - \boldsymbol{q}) + \boldsymbol{B}(\dot{\boldsymbol{q}}_0 - \dot{\boldsymbol{q}}) \quad (2)$$

The stiffness in units of N·m/rad was defined as

$$\boldsymbol{K} = G\begin{bmatrix} K_{11} & K_{12} \\ K_{21} & K_{22} \end{bmatrix} = G\begin{bmatrix} 29.5 & 14.3 \\ 14.3 & 39.3 \end{bmatrix} \quad (3)$$

The viscous damping in units of N·m·s/rad was defined as

$$\boldsymbol{B} = \begin{bmatrix} B_{11} & B_{12} \\ B_{21} & B_{22} \end{bmatrix} \quad (4)$$

where K_{11} and B_{11} are the net shoulder joint stiffness and damping; K_{12}, B_{12}, K_{21}, and B_{21} are the two-joint parameters, and K_{22} and B_{22} describe the elbow parameters; G is a dimensionless scalar. The values for joint stiffness and damping were similar to those of Flash (1987), such that $\boldsymbol{B} = \beta\boldsymbol{K}$. The β term had units of time, consistent with a first-order model of muscle impedance (Hill 1938). A gain of $G = 0.5$ was used in the slow and medium cases, and a gain of $G = 1.5$ was used in the fast case. Damping was derived from stiffness by multiplication by a constant factor, β, which was 0.05 s for the slow and medium cases, and 0.1 s for the fast cases.

Substituting *Eq. 2* into *Eqs. A2*, *A3*, and *A4* (from APPENDIX A), the equation could be manipulated to solve for $\dot{\boldsymbol{q}}_0$:

$$\dot{\boldsymbol{q}}_0 = \boldsymbol{B}^{-1}\Big\{\boldsymbol{M}\boldsymbol{J}^{-1}\Big[\big(\boldsymbol{J}\boldsymbol{M}^{-1}\boldsymbol{J}^T + r^2 I^{-1}\boldsymbol{e}\boldsymbol{e}^T\big)\boldsymbol{F} - \dot{\boldsymbol{J}}\dot{\boldsymbol{q}} - r\dot{\theta}\big(\dot{\theta}\boldsymbol{n} + b_c I^{-1}\boldsymbol{e}\big)\Big] + \boldsymbol{h} - \boldsymbol{K}(\boldsymbol{q}_0 - \boldsymbol{q})\Big\} + \dot{\boldsymbol{q}} \quad (5)$$

Integrating *Eq. 5* allowed for the computation of the zero-force trajectory corresponding to a prescribed position, velocity, acceleration, and force.

The velocity and force signals were filtered with a second-order, zero-phase-lag Butterworth filter using a cutoff frequency of 10 Hz, except in the slow condition, as the tangential force in the slow condition was small in magnitude. At slow speeds, a large number of samples with a magnitude close to the resolution of the sensor was observed. This resulted in artifactual step changes in the force measurements. To eliminate this artifact, the tangential force in the slow condition was filtered with a cutoff frequency of 0.5 Hz, far faster than the turning frequency of the slow task (0.075 rev/s).

Speed-Curvature Relation

In unconstrained motions, the relation between curvature and speed has been well documented in human arm trajectories. This study investigated if this relation was evident in the zero-force trajectory. To compute the speed and curvature of the zero-force trajectory, it was transformed into Cartesian coordinates, x_0 and y_0. Using the methods of Dohrmann et al. (1988), the derivatives of the Cartesian position of the zero-force trajectory were computed. Smoothing parameters of 10^{-3}, 10^{-7}, and 10^{-11} were used for the slow, medium, and fast trials, respectively. These derivatives were used to compute tangential speed, V_0, and curvature, κ_0

$$V_0 = \sqrt{\dot{x}_0^2 + \dot{y}_0^2} \quad (6)$$

$$\kappa_0 = \frac{\dot{x}_0\ddot{y}_0 - \dot{y}_0\ddot{x}_0}{(\dot{x}_0^2 + \dot{y}_0^2)^{3/2}} \quad (7)$$

Positive curvature would be consistent with a positive z rotation, according to the right-hand rule. However, for ease of computation, the radially inward direction was defined as positive curvature.

Previous reaching studies have shown that, when curves more complex than simple ellipses were investigated, the simple power-law relation between speed and curvature was not observed. Instead, a more complex pattern emerged that could be characterized by a "spectrum of power laws" (Huh and Sejnowski 2015). However, the temporal coincidence of extrema of speed and curvature was retained in all cases. The original study by Abend et al. (1982) and, to the best of our knowledge, all related studies since then have observed this temporal coincidence. The present study examined the data for this temporal coincidence. To this end, local minima in tangential speed and local maxima in curvature were identified, and their temporal relation was quantified. For each local minimum in tangential speed, the nearest local maximum in curvature was found. The signed distance between the two extrema was normalized by the target speed and defined as the interval Δ. This metric was computed for each trial in each condition, and the data were pooled across trials for each subject. The 95% confidence interval of the mean for each subject in each condition was computed.

Sensitivity to Impedance Assumptions

To the best of our knowledge, limb impedance measurements during physical interaction with a constraint have not been reported. Thus impedance parameters were based on unconstrained static arm stiffness and single joint damping measurements. Consequently, the impedance parameters, the gain term for the stiffness, G, and the proportional damping term, β, were varied to understand if the results were sensitive to the impedance values used to compute the zero-force trajectory. When the gain and damping terms changed, the zero-force trajectory was expected to change. However, the main question was whether any speed-curvature relation was affected when the zero-force trajectory changed shape. To this end, the 95% confidence interval of the mean for Δ was computed when the G and β terms were each varied over a 3:1 range.

RESULTS

Speed and Force at Preferred Speed

The preferred speed trials were collected to establish a baseline and quantify human performance without visual feedback. A representative subject's turning speed and normal force are plotted with respect to crank angle in Fig. 3. His speed fluctuated about 0.5 rev/s, and systematic variations with angular position were evident (Fig. 3, *top*). Furthermore, the subject's force alternated between tension (positive) and compression (negative), depending on the crank angle (Fig. 3, *bottom*). Some minor differences appeared between the two turning directions.

Despite the appearance of occasional differences between CW and CCW performance, the population means of speed did not show any statistically significant differences between the CW (0.37 ± 0.11 rev/s), and CCW (0.40 ± 0.10 rev/s) conditions ($P = 0.539$). There was also no significant difference between mean normal force in the CW (-0.58 ± 1.65 N), and CCW (-0.12 ± 1.43 N) conditions ($P = 0.462$). Furthermore, the mean normal force was not significantly different from zero in the CW condition ($P = 0.325$, $\alpha_{SID} = 0.0253$), or CCW condition ($P = 0.811$, $\alpha_{SID} = 0.0253$). Figure 4 displays these dependent measures as a function of mean speed, with each point representing the subject average of all trials per condition. This figure illustrates the lack of discernible differences between the two rotation directions.

Speed and Force at Instructed Speeds

In these trials, subjects were instructed to turn at one of three speeds, in both CW and CCW directions, with visual feedback provided. Before all subsequent analyses, the data were screened for any learning effects. We found no evidence of

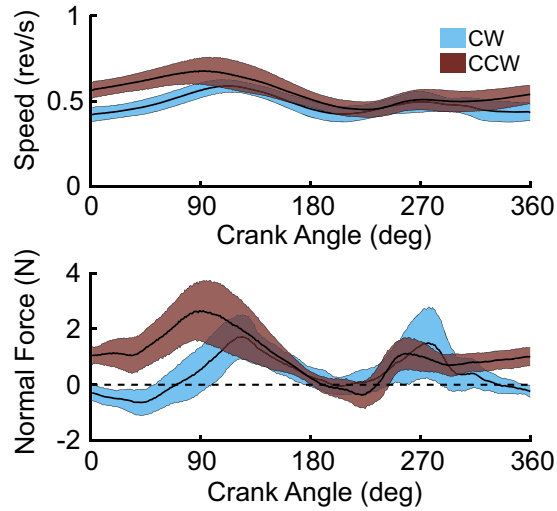

Fig. 3. Representative data from one subject's tangential speed (*top*) and normal force (*bottom*) with respect to crank position at comfortable speed. Blue lines indicate clockwise (CW) trials, and brown lines indicate counterclockwise (CCW) trials. Each line represents binned speed or force values for 1 of the 10 trials. The shading indicates 1 SD from the mean across trials.

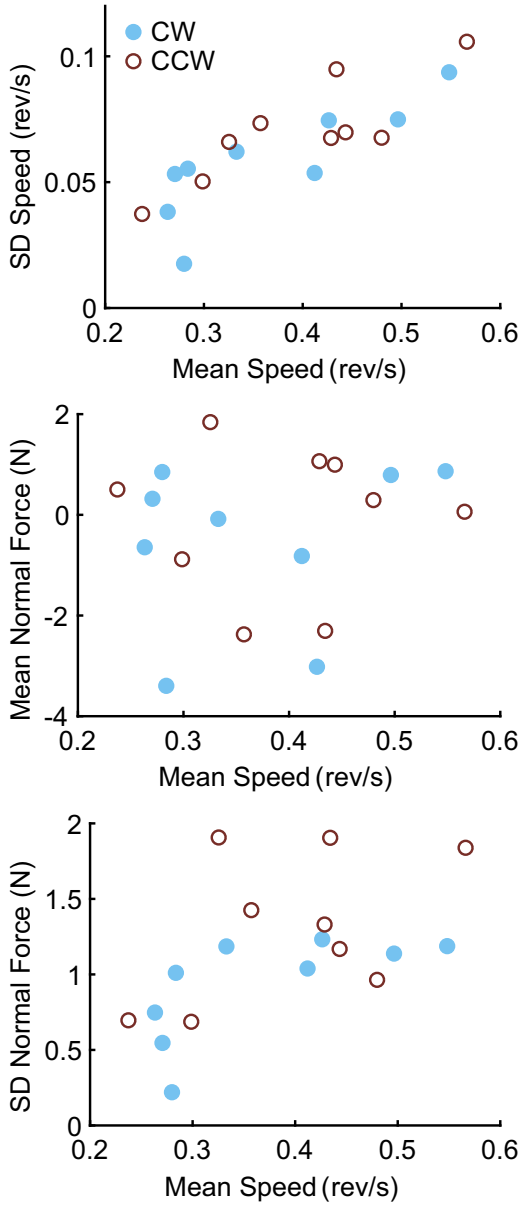

Fig. 4. Dependent measures with respect to mean speed for preferred speed trials: SDs of speed (*top*), mean normal force (*middle*), and SDs of normal force (*bottom*). Blue dots: clockwise direction (CW); brown circles: counterclockwise direction (CCW).

learning over the duration of the experiment reported in this study. Linear regressions of all dependent measures, including mean and SD of speed and force, yielded regressions with R^2 values < 0.10. Figure 5 shows mean speed and force of all subjects with respect to crank angle for the slow, medium, and fast conditions. Each line represents the mean across all subjects, and the shadow band represents 1 SD around the mean. The figure reveals a noticeable pattern with respect to crank angle in the two dependent measures.

Figure 6 summarizes mean and SD of speed and normal force for the three different target speeds and two directions. The four dependent measures were analyzed with respect to the experimental conditions, speed and direction. Mean speed showed only a main effect of target speed ($F_{2.0,18} = 3579.51$, $P < 0.001$), indicating that, as expected, subjects could successfully perform this task. Mean speed showed no main effect of direction nor any interaction. The SD of speed showed a significant interaction between speed and direction ($F_{2.0,18} = 5.32$, $P < 0.015$) and a main effect of speed ($F_{2.0,18} = 477.50$, $P < 0.001$). Post hoc pairwise t tests identified significant differences between CW and CCW at the medium and fast speeds, as well as the evident differences between slow, medium, and fast speeds. Figure 6 shows that the interactions, while significant, were negligible in magnitude. Thus target speed was the predominant factor influencing the mean and SD of speed.

Analysis of the mean normal force (Fig. 6, *bottom left*) revealed a significant interaction between speed and direction ($F_{2.0,18} = 3.75$, $P = 0.043$), and a main effect of target speed ($F_{2.0,18} = 258.88$, $P < 0.001$). There was no significant effect of direction. Post hoc pairwise t tests identified a significant difference between CW and CCW at the fast speed. Additionally, significant differences were identified between the slow, medium, and fast speeds for both directions. The large difference between the medium and fast conditions was clear, whereas the significant difference between the slow and medium speeds was less pronounced. As above, we regarded the interactions as negligible. Lastly, analysis of the SD of normal force revealed only a significant main effect of speed ($F_{2.0,18}$=749.292, $P < 0.001$). Target speed was the predominant factor influencing the mean normal force.

In the instructed speed trials, occasional catch trials occurred in which visual feedback was withheld. Comparing the dependent measures for the catch trials and the immediately preceding trials with visual feedback assessed whether visual feedback affected subject performance. Three-way ANOVAs were conducted for all dependent measures. These comparisons resulted in several significant interactions, including three-way interactions. However, this reflected the strength of the statistical analysis rather than the magnitudes of these effects, which were negligible (see APPENDIX B).

Zero-Force Trajectory

The bidirectional interaction between the forces exerted on the constraint and the force observed at the hand was described by mechanical impedance. A model of upper-limb mechanical impedance was assumed, and the zero-force trajectory (defined above) was computed. Figure 7 shows one example from a representative subject in the three speed conditions in the *left* panels; the *right* panels shows the mean trajectories from all subjects. The black dashed circle is the circular path of the crank. It is clear in all subjects that the zero-force trajectory deviated from the circular path, both closer to and further from the center of the crank circle, and was roughly elliptical. Furthermore, the speed of the zero-force trajectory, shown by the color gradient, varied systematically along the elliptical path. Visually, the regions of high speed corresponded well to the regions with low curvature and vice versa. This observation motivated a test of the hypothesis that a systematic speed-curvature relation is found in the motion consequences of neural activity.

To test this relation quantitatively, the extrema of speed and curvature were determined, and the difference in crank angle between speed and curvature extrema Δ was computed. Exact temporal coincidence would lead to zero Δ values. Figure 8

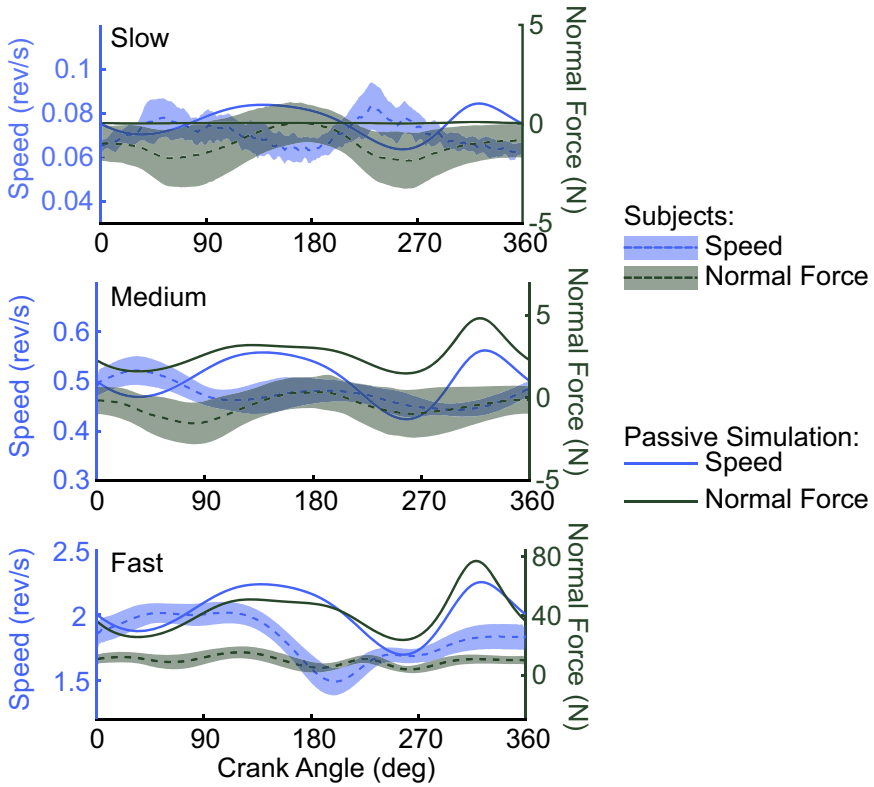

Fig. 5. Mean and SDs of speed (blue dashed line) and normal force (green dashed line) versus crank angle for all subjects. The shading indicates 1 SD from the mean across subjects. Data are from the clockwise direction trials. Note the different scales on the ordinates. Simulation results are included as solid lines to illustrate the fluctuations resulting from passive inertial mechanics: fluctuations of speed (blue) and normal force (green). At the slowest speed, the normal force due to passive inertial mechanics is indistinguishable from zero because it did not exceed a magnitude of 0.11 N.

shows representative profiles of the speed and curvature of the zero-force trajectory for a single trial performed by one subject at each of the three speed conditions in the CW direction. The circles at the extrema highlight that the minima in the speed profile are in close temporal vicinity of the maxima of curvature. The data of the same subject from Fig. 7 are summarized in the histograms for the three speed conditions. The 95% confidence intervals of the mean for the Δ parameter of all subjects in the six conditions were less than 3% of a revolution, indicating that the curvature peaks corresponded to the speed

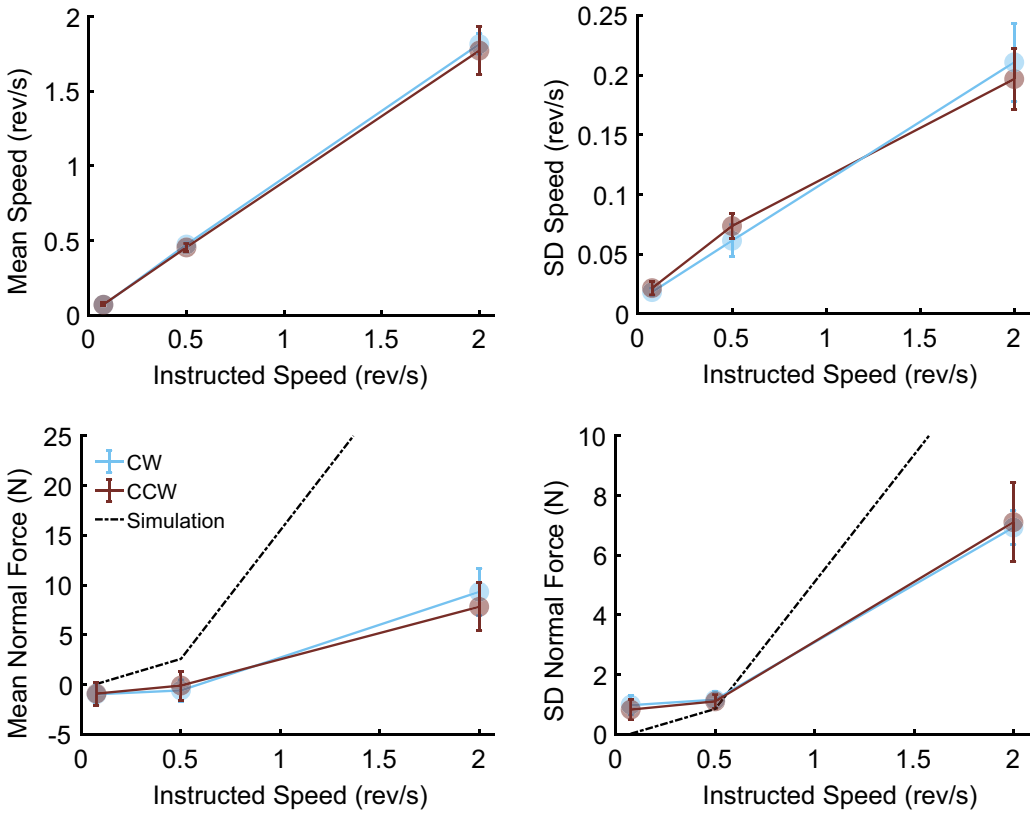

Fig. 6. Dependent measures mean speed, SD speed, mean normal force, and SD normal force. Error bars indicate 1 SD across subjects. Clockwise (CW) trials are depicted in blue, and counterclockwise (CCW) trials are in brown. The black dashed lines in the *bottom* two panels indicate the fluctuations that result from only inertial effects. As inertial dynamics does not vary with direction, there is only one line for the simulations.

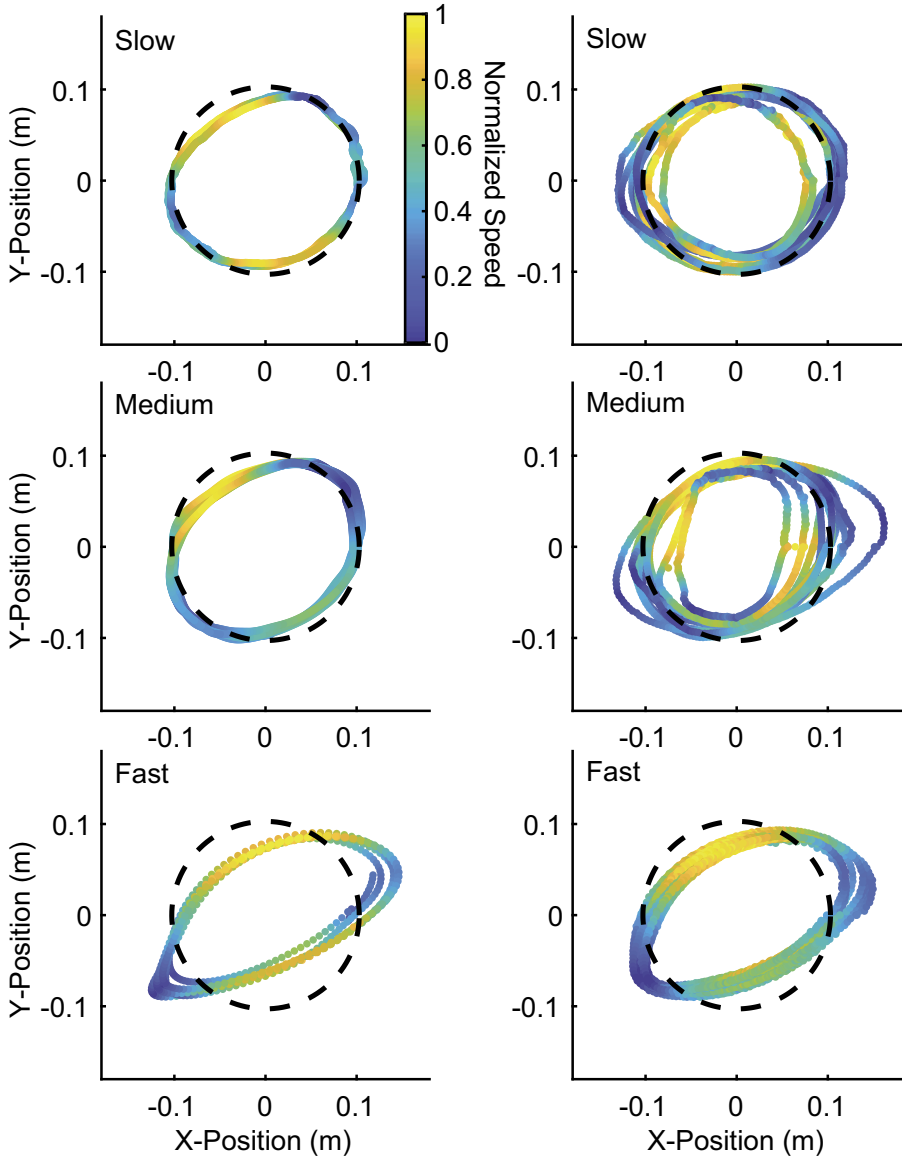

Fig. 7. *Left*: one representative trial from one subject in each of the speed conditions. *Right*: average zero-force trajectories for all 10 subjects for each speed condition. *Top*: slow speed; *middle*: medium speed; *bottom*: fast speed. The plots are from the clockwise direction trials. The path defined by the constraint is shown by the black dashed circle. The zero-force trajectories are shown with variable color lines. Color indicates speed along the zero-force path normalized by its range.

valleys. Figure 9 displays the 95% confidence intervals of the mean of the Δ parameter for all 10 subjects. This result recapitulates observations of unconstrained hand motion.

Sensitivity Analyses of the Zero-Force Trajectory and its Effect on the Speed-Curvature Relation

The zero-force trajectory is a construct derived from our experimental observations based on several assumptions combined with parameter values from the published literature. To assess the sensitivity of this construct to the assumptions used to compute it, key parameters of the model were varied over a 3:1 range. A linear time-invariant first-order model of mechanical impedance was assumed, with damping proportional to the assumed stiffness. Values for the gain term G were [0.25, 0.50, 0.75] (slow and medium), and [0.75, 1.50, 2.25] (fast); values of the proportionality constant β were [0.025 s, 0.05 s, 0.075 s] (slow and medium), and [0.05 s, 0.1 s, 0.15 s] (fast). We anticipated that, if the impedance was varied, the zero-force trajectory would change, and it did (see APPENDIX C). Nevertheless, the coincidence of the curvature and speed extrema was still observed, even when the zero-force path changed shape. The 95% confidence interval of the mean of Δ was always less than 4% of a revolution from zero. Hence, the coincidence between curvature and speed extrema was not sensitive to the particular values of stiffness and damping, and the observed results were robust.

DISCUSSION

Long-standing experience in robotics has shown that physical interaction is challenging (Colgate and Hogan 1989, 1988; Paul 1987; Whitney 1977). Specifically, contact with a kinematic constraint may compromise both dynamic and static stability (Rancourt and Hogan 2001, 2009). It is, therefore, quite remarkable that humans do not display any sign of instability in tasks such as opening a door or turning a crank. In fact, this discrepancy highlights a more general issue and challenge in the study of motor control: observations of biology disguise the control problems that have been solved because unsuccessful strategies tend to leave the gene pool. In contrast, engineering studies make some problems obvious

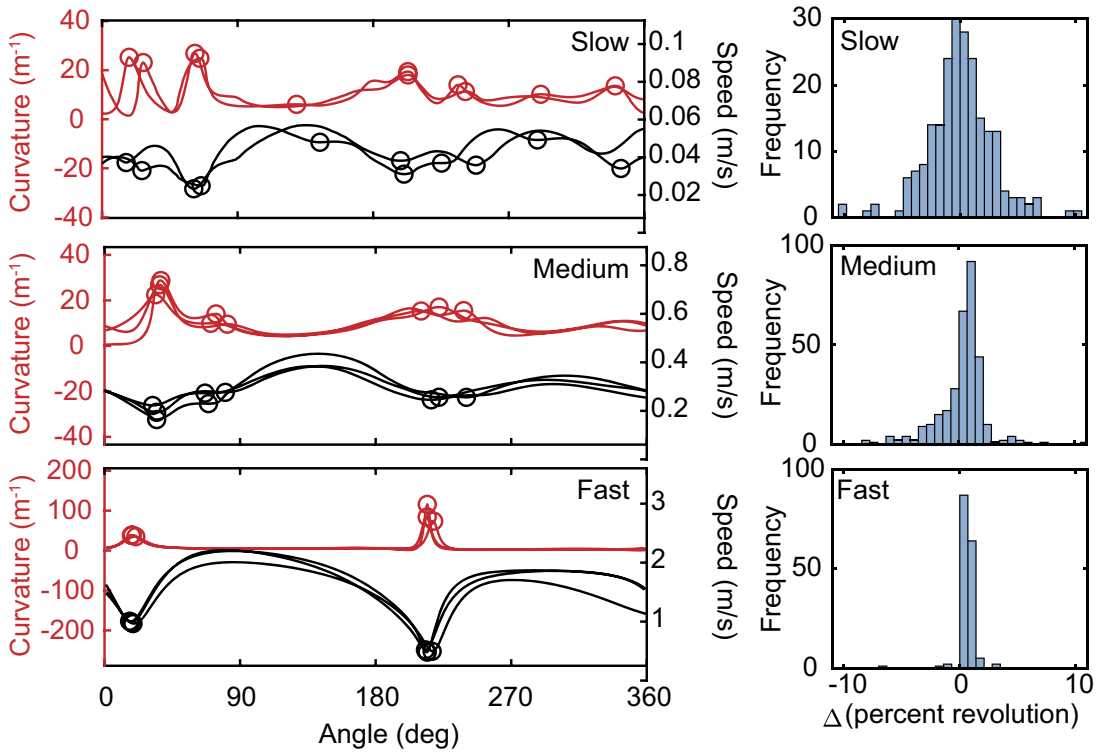

Fig. 8. *Left*: zero-force trajectory speed (black) and curvature (red) for a single trial performed by one representative subject at each of the three speed conditions in the clockwise direction. *Top*: slow speed; *middle*: medium speed; *bottom*: fast speed. The circles highlight the extrema in both profiles. *Right*: histograms of Δ for all trials performed by this representative subject at each of the three speed conditions in the clockwise direction.

(machines often do not work as planned), although their solutions may be obscured. A combined approach, drawing on both engineering and biology, promises superior insight.

The present study examined how humans managed physical interaction with a kinematic constraint by investigating their patterns of motion and force while turning a crank. This action is typical of many activities of daily living that humans perform with ease, with no evidence of the instability that robots typically exhibit. However, it has been proven that properties of interactive dynamics (mechanical impedance) afford a general solution to the stability problem: coupled stability is guaranteed if mechanical impedance mimics that of an energetically passive object (Colgate and Hogan 1989, 1988). Studies of human limb impedance show that it appears to have this property (Lee et al. 2014a, 2014b). Clearly, mechanical impedance is an important aspect of peripheral neuromechanics and must be taken into account if we wish to disentangle peripheral neuromechanics from central control.

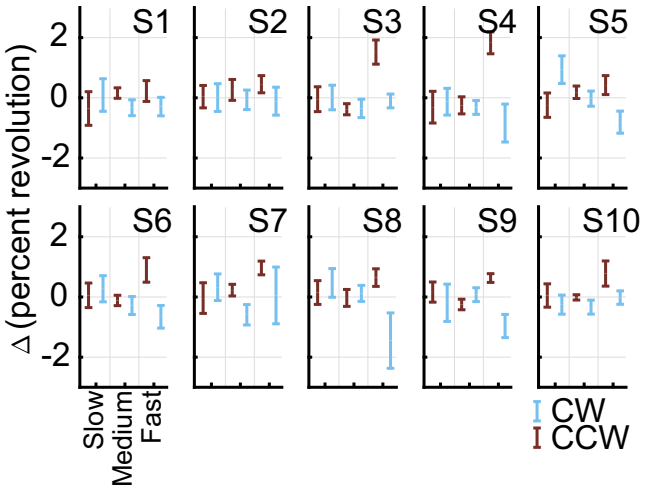

Fig. 9. 95% confidence intervals of the mean of Δ for all 10 subjects (S1–S10) in each speed and direction. Confidence intervals are grouped by speed, and the color indicates turning direction [blue: clockwise (CW), and brown: counterclockwise (CCW)].

That is the motivation behind the construct that we have called the zero-force trajectory. It is the motion that would have occurred if the peripheral mechanics and external forces were not present. By definition, the zero-force trajectory is a summary of one aspect of the underlying neural commands, expressed in terms of motion. Even though the hand path is circular, i.e., of constant curvature, the zero-force trajectory may not be exactly circular. In that case, if the speed-curvature relation is of neural origin, we would expect it to reemerge in the zero-force trajectory. Our results, in fact, showed that a speed-curvature relation observed in unconstrained movements reemerged in the zero-force trajectory.

Even if stability is assured, if the action is controlled in terms of motion, negotiating a constraint may require detailed knowledge of the constraint and precise musculoskeletal coordination. Evidence from reaching studies suggests that the control of unconstrained hand motion involves some form of internal model. That model includes kinematics, relating hand position to joint angle or muscle length, and dynamics (of at least the musculoskeletal system), relating muscle force to hand motion (Kluzik et al. 2008; Lackner and Dizio 1994; Wolpert et al. 1995, 1998). However, constrained motion introduces a "closed chain" that changes both the kinematic and dynamic models and makes them much more challenging (Slotine and Asada 1992).

In robotics, one proposed approach to constrained motion is "hybrid control": parse the work space into independent directions and control force when motion is zero, i.e., normal to a constraint, and control motion when force is zero, i.e., tangent

to a constraint (Khatib 1987; Mason 1981; Raibert and Craig 1981). While consistent with recent work by Chib et al. (2009), it requires precise knowledge of the constraint to identify the normal and the tangent. Such precision in human movement control seems implausible. Instead, humans may exploit the "softness" of neuromuscular mechanical impedance to reduce the required knowledge and precision. Our experiments were designed to explore the plausibility of such a simplified approach. For that reason, this disarmingly simple task may provide significant insight about how humans manage more sophisticated tools.

Two previous studies investigated pen tracing on the inner edge of a template (Catavitello et al. 2016; Lacquaniti et al. 1983). Catavitello and colleagues reported differences in the speed-curvature relation during drawing motions performed in air versus in water. They suggest that the dynamics of the limb itself must be considered. Unlike the present study, these were "half-space" constraints, which required nonzero unidirectional normal force. Here we considered the more common case of a constraint that could (in principle) be negotiated with zero normal force, consistent with "hybrid control." In this case, deviations from zero normal force are particularly informative.

Patterns of Speed and Force

When subjects turned the crank at their preferred rate, small fluctuations of speed about a mean value were observed. Normal force fluctuated about zero, and both varied systematically with crank angle, consistent with previous work (Ohta et al. 2004; Russell and Hogan 1989). The direction of rotation had no significant effect on the means of these measures. When subjects moved at a mean speed guided by a visual target, fluctuations of speed and normal force that varied systematically with crank position were again observed. To test the influence of visual feedback, we compared the dependent measures of the catch trials (in which visual feedback was removed) with the immediately preceding trials. While some statistically significant differences were observed, they were negligibly small. We concluded that removing visual feedback had no substantial effect.

Might these fluctuations reflect imperfect compensation for musculoskeletal dynamics? Inertial forces increase with the speed of crank rotation, with a concomitant increase of muscle force and hence muscle noise. Consistent with imperfect compensation, the SDs of speed and normal force both increased with instructed speed. To test whether the systematic variation of speed and force with crank angle might also be due to imperfect compensation, simulations of the passive inertial dynamics of the arm constrained by the crank, but with no muscle action, were performed. These simulations exhibited systematic variation of both force and speed with crank angle, but with patterns that could not account for our observations. At the fast and medium speeds, the magnitudes of simulated normal force were greater than observed, indicating that subjects partially compensated for inertial effects. Most notably, at the slowest speed, the simulated normal force was essentially zero. In fact, this was one reason why such a slow speed (over 13 s per revolution) was chosen. In contrast, the pattern displayed by human subjects was quite different (Fig. 5). This indicated that incorrect compensation for inertial dynamics was not the cause of the observed fluctuations in speed and normal force.

The Zero-Force Trajectory

The zero-force trajectory is a construct based on measured force and motion, combined in a model of peripheral neuromechanics. It allows us to "peel back" the peripheral neuromechanics to uncover one consequence of the underlying neural commands, and that consequence is expressed in terms of motion. It is similar to, but distinct from, the virtual trajectory of the equilibrium-point hypothesis (Bizzi et al. 1982, 1984; Feldman 1966, 1986). That is because the forward-path dynamics between neural input and actual motion is, in general, quite different from the interactive dynamics (mechanical impedance) used to construct the zero-force trajectory. Because of neural transmission delays, excitation-contraction coupling and other dynamic effects in the forward path, the zero-force trajectory may differ from the virtual trajectory (Gribble et al. 1998). More importantly, unlike the virtual trajectory, we remain agnostic about whether the central nervous system actually encodes the zero-force trajectory. It is an observation defined by measurements of hand force and motion combined with an estimate of interactive dynamics. However, while it reflects a consequence of neural activity, it is unknown whether this quantity is represented in higher-level activity of the central nervous system. Similarly, an actual unconstrained trajectory is also a consequence of neural activity, but observation of an actual trajectory is not sufficient to determine how neural activity controls or encodes this quantity; nevertheless, observations of actual motion have proven to be informative. The zero-force trajectory is a way to interpret measured force and motion, in combination with a reasonable, albeit simplified, model of peripheral neuromechanics. As with actual unconstrained trajectories, we believe observations of the zero-force trajectory are informative.

If the exact neuromechanical impedance were known for each subject, this construct would be an exact (i.e., noise-free) measure of the motion consequences of neural commands. However, as we used average measures of neuromechanical impedance obtained from different subjects and during static conditions, this construct is at best a noisy and uncertain estimate based on a number of assumptions. It assumed a model of neuromuscular dynamics that is time invariant, first order, and linear. All of these assumptions are questionable, or even demonstrably incorrect, but they served as workable approximations. The most critical assumptions used to compute the zero-force trajectory were that impedance was linear and time invariant, with a constant stiffness and damping in joint coordinates. Linearization is valid if the actual (nonlinear) interactive dynamics are differentiable, and deviations from the linearization operating point are small. The proximity of the zero-force trajectory to the circular constraint path suggests that the linear approximation was reasonably accurate. The time-invariant parameters were based on measurements made under static postural conditions (Flash 1987; Mussa-Ivaldi et al. 1985). The slow speed condition was quasi-static, close to postural conditions. Therefore, the elliptical zero-force path seen in this condition was least sensitive to the assumption of time invariance. The analysis also assumed that stiffness and damping were symmetric, proportional to each other, con-

nected with a specific topology,[1] and that the same values of stiffness and damping could be applied to all subjects. The assumptions of symmetric stiffness and damping coefficients may be justified, as this is sufficient to ensure a stable interaction (Colgate and Hogan 1988). Moreover, the study from which we derived the stiffness parameters also reported a symmetric stiffness. The proportionality between stiffness and damping implies first-order interactive dynamics, consistent with experimental observations (Hill 1938). However, it also implies that a single time constant describes the interactive dynamics of all muscles contributing to the overall mechanical impedance.

Given the uncertain and approximate nature of these assumptions, the regularity of the pattern that emerged is striking. Unlike the findings of Gomi and Kawato (1996), our analyses yielded a zero-force trajectory close to the actual hand path, consistent with the work of Won and Hogan (1995). In addition, the statistical reliability of our estimates is quite remarkable, even though we varied the impedance parameters over a 3:1 range. It suggests that, from macroscopic behavioral measurements, we can approximate at least some consequences of the underlying neural processes, i.e., that behavior can be informative about underlying neural processes (Krakauer et al. 2017).

Speed-Curvature Relation in the Zero-Force Trajectory

In a study of unconstrained two-joint upper-limb reaching, Abend et al. (1982) reported that human hand trajectories exhibited a coincidence between curvature maxima and speed minima: speed decreased when the curvature increased. When studied in explicitly elliptical trajectories, the speed-curvature relation was described by a two-thirds power law (Lacquaniti et al. 1983), such that the relation between instantaneous angular velocity, $A(t)$, and the curvature, $C(t)$, was expressed as $A(t) = K_C C(t)^{2/3}$, where K_C is a constant (the so-called velocity gain factor). The law can also be written in terms of a one-third power law relating the instantaneous tangential velocity, $V(t)$, and the radius of curvature, $R(t) = 1/C(t)$, and expressed as $V(t) = K_R R(t)^{1/3}$, where K_R is a constant. For this reason, it is often referred to as the two-thirds or one-third power law, respectively.

This power law was reported for drawing ellipses and several other geometric figures (such as lemniscates); however, the reason for this relation was not clear. Viviani and Terzuolo (1982) originally suggested it to result from central computational constraints, which occur during the translation of movement trajectories into the appropriate motor parameters. However, others showed that this relation might simply emerge as a result of neuromechanics or oscillatory movements in joint space (Gribble and Ostry 1996; Schaal and Sternad 2001; Sternad and Schaal 1999). Intuitively, it makes sense that the limb slows down when accelerating around a corner, because the arm is an inertial body actuated by muscles: finite force actuators with limited stiffness. Using the lambda-equilibrium-point model, Gribble and Ostry (1996) generated an input command that did not follow a speed-curvature relation. Nevertheless, the simulated motion exhibited a speed-curvature relation. When testing the alpha-equilibrium-point model as simulated by Flash (1987), they observed the same result. In other work, Schaal and Sternad (Schaal and Sternad 2001; Sternad and Schaal 1999) showed that a power-law relation between hand speed and curvature relation emerges from simple oscillatory joint motions in a 7-degrees-of-freedom arm model. This was motivated by the fact that two sinusoids of the same frequency but with different phases, as in a Lissajous plot, produce the power-law behavior exactly. More importantly, this account predicted systematic deviations from a power-law relation for large motions, which were confirmed by experimental observation.

Other observations across multiple tasks and extremities, as well as in the perception of actions, provided evidence that the power-law relation is of nonmechanical, i.e., neural origin (Dayan et al. 2007; Hicheur et al. 2005; Maurice et al. 2018b; Viviani and Flash 1995). For example, Massey et al. (1992) performed an experiment where subjects grasped a three-dimensional isometric force-sensing handle and exerted forces continuously to draw circles, ellipses, and lemniscates on a screen, with and without visual feedback. The power-law speed-curvature relation was observed even when the hand did not move, indicating that inertial dynamics alone could not be its cause. Nevertheless, a later study by Gribble and Ostry (1996) showed that biomechanics may account for a speed-curvature relation, even during isometric conditions. Other research has shown that movement production involves the cooperative interaction of large neuronal populations (Georgopoulos et al. 1986). Schwartz (1994) used a population vector method to interpret one aspect of neural activity as representing spatial motions. This information was then used to visualize motor cortical representations of wrist trajectories, which were remarkably similar to the actual wrist motions made by monkeys as they drew spirals. Surprisingly, a power law relating speed and curvature was observed in this cortically derived representation of motion. Neuromechanics alone cannot account for these observations.

A possible resolution of this controversy is that the neural controller and the neuromechanical periphery coevolved to embody similar dynamic structures and constraints. Long communication delays are a core challenge of human motor control. Coping with these delays requires a controller that favors predictability, even over energetic cost in some cases (Bazzi et al. 2018; Koeppen et al. 2017; Maurice et al. 2018a; Nasseroleslami et al. 2014; Sternad and Hasson 2016). Smoothness quantified by minimizing mean-squared jerk provides a measure of predictability, and maximizing smoothness has been shown to account for the coordination of simple reaching movements, including an account for the two-thirds power law (Flash and Hogan 1985; Richardson and Flash 2002; Schaal and Sternad 2001; Sternad and Schaal 1999; Viviani and Flash 1995). More recent work by Huh and Sejnowski (2015) showed that maximizing smoothness along a curved path yields a spectrum of power-law speed-curvature relations.

Periodic actions are (in principle) infinitely predictable and have been proposed as one class of dynamic primitives used to construct motor behavior (Hogan 2017; Hogan and Sternad 2012, 2013; Ronsse et al. 2009; de Rugy and Sternad 2003; Schaal and Sternad 1998; Sternad 2008; Sternad et al. 2000). An elliptical path may be generated by combining two sinusoids of the same frequency at a nonzero relative phase, although possibly of different amplitudes. The resulting trajec-

[1] In this context, "topology" refers to how the stiffness and damping are connected in the model.

tory (i.e., time course of speed along the elliptical path) necessarily exhibits a power-law relation between speed and curvature. Generating an elliptical zero-force trajectory via out-of-phase sinusoids is consistent with our observations. The same model (a zero-force trajectory composed of simple dynamic primitive oscillations) may account for the observations of Massey et al. (1992) and possibly those of Schwartz (1994). Perhaps more important, it is also consistent with prioritizing predictability over other aspects of performance, including the variability of actual hand speed and exerted normal force.

Conclusion

Unconstrained curved movements exhibit a systematic relation between speed and curvature. This has been attributed to either neural or mechanical causes, without resolution of the debate. To obtain a new perspective on this open question, this study examined movements against a simple kinematic constraint. By design, the experiment confined the hand to a circular path with constant curvature; speed was controlled by instruction with visual feedback. If control in constrained motion is focused on hand trajectories, there should be no reason for a systematic variation of speed as curvature was constant. Nevertheless, systematic fluctuations of speed and normal force were observed at all speeds, unaffected by the presence or absence of visual feedback. When the influence of peripheral neuromechanics was subtracted based on a biomechanical model to identify a zero-force trajectory, an elliptical shape emerged that exhibited the widely observed relation between speed and curvature extrema: Extrema of curvature and tangential speed were systematically time aligned. This relation persisted even when the stiffness and damping parameters of the model were varied over a wide range. These findings provide evidence that the speed-curvature relation is due, at least in part, to neural processes, possibly reflecting their co-evolution with peripheral dynamic structures. These results are also a first demonstration that the zero-force trajectory may successfully disentangle neural and biomechanical factors underlying motor actions.

APPENDIX A: MODELING A TWO-LINK MANIPULATOR COUPLED TO A CRANK

Knowledge of the subject's inertia is required to develop a model and simulate the system. Inertia parameters were estimated based on the results of the cadaver studies of Dempster (Miller and Nelson 1973; Plagenhoef 1971). The arm and forearm plus hand were denoted by *links 1* and *2*, respectively. Each of the body segments was described by the following parameters: length, l; mass, m; inertia, I; and center of mass, c. The length l_1 was the distance from the shoulder to the elbow. The length l_2 was the distance from the elbow to the center of the fist. *Link 2* was considered a combination of the forearm and hand. The hand was assumed to be a point mass at the end of the forearm. Limb parameters are reported in Table A1. The inertia of the crank about the pivot was 3.716×10^{-3} kg/m^2. Analysis of the mean and median of all subjects' inertial parameters showed that *subject 1* was representative (Doeringer 1999).

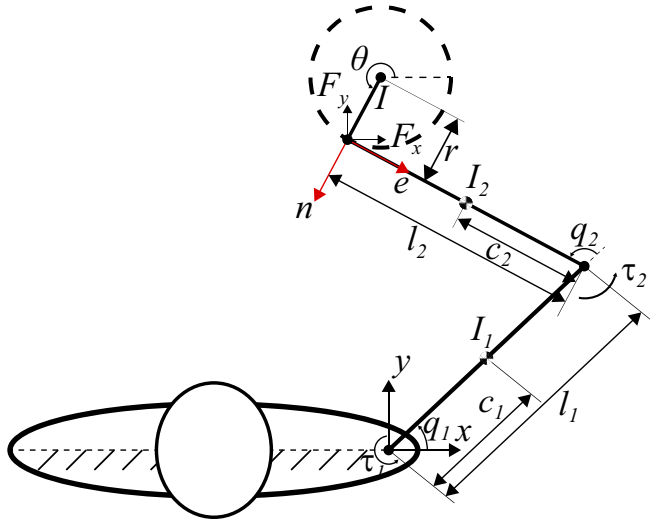

Fig. A1. Model of crank rotation task that displays the sign convention and notation used in the computations. See APPENDIX A for definitions of terms.

The model of the arm and crank system was constructed in the same manner as performed by Ohta et al. (2004). Figure A1 displays the variables and notation used in the development of the model. The system has one degree of freedom; therefore, there is always a kinematic relation that can be used to transform from Cartesian position, $\boldsymbol{x} = [x,y]^T$, to joint position, $\boldsymbol{q} = [q_1,q_2]^T$, and to crank position, θ, where the center of the crank is defined as $\boldsymbol{x}_c = [x_c,y_c]$.

$$\boldsymbol{x} = \begin{bmatrix} l_1C_1 + l_2C_{12} \\ l_1S_1 + l_2S_{12} \end{bmatrix} = \begin{bmatrix} r\cos\theta \\ r\sin\theta \end{bmatrix} = \boldsymbol{x}_c \qquad (A1)$$

The notations S_1, C_1 denote $\sin(q_1)$, $\cos(q_1)$ and S_{12}, C_{12} denote $\sin(q_1 + q_2)$, $\cos(q_1 + q_2)$. The radius of the crank is r, the damping of the crank is b_c, and the inertia is I. The arm denoted subscript 1 and the forearm denoted subscript 2 are described by length l_1, l_2; mass m_1, m_2; inertia about the z axis I_1, I_2; and center of mass distance from the joint axis c_1, c_2. The force on the handle is $\boldsymbol{F} = [F_x,F_y]^T$, with the

Table A1. *Human limb inertia properties for this experiment*

Subject No.	l_1, cm	c_1, cm	m_1, kg	I_1, kg/m^2	l_2, cm	c_2, cm	m_2, kg	I_2, kg/m^2
1	36.8	16.1	2.23	0.0313	37.5	23.6	2.25	0.0440
2	36.2	15.8	2.03	0.0276	36.8	23.6	2.10	0.0395
3	32.4	14.1	2.20	0.0239	33.0	20.7	2.23	0.0340
4	36.2	15.8	2.61	0.0354	38.1	23.5	2.55	0.0515
5	34.9	15.2	2.03	0.0257	35.6	22.7	2.10	0.0369
6	29.2	12.7	2.35	0.0208	33.7	20.8	2.35	0.0375
7	37.5	16.3	1.97	0.0287	37.5	24.0	2.05	0.0401
8	34.3	15.0	1.97	0.0240	36.8	23.7	2.05	0.0385
9	36.8	16.1	2.03	0.0286	38.7	24.9	2.10	0.0435
10	34.3	15.0	2.29	0.0279	33.7	21.1	2.30	0.0364

1, Arm; 2, forearm; l, length; c, center of mass distance from the joint axis; m, mass; I, inertia about the z axis.

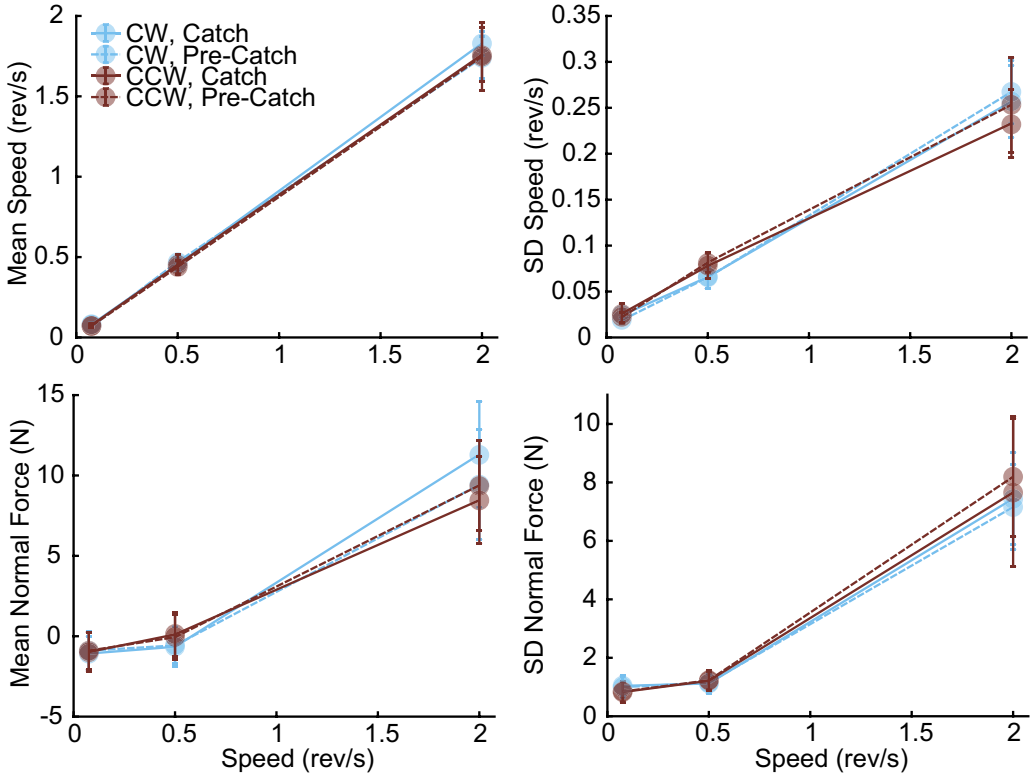

Fig. B1. Mean and SDs (*top*) of speed and mean and SDs of normal force (*bottom*) for the three speed conditions; error bars indicate the SDs across the 10 subjects; clockwise (CW) trials are depicted in blue, counterclockwise (CCW) trials are in brown. The brown solid lines represent the catch trials (where visual feedback was withheld), the brown dashed lines represent the trials immediately before the catch trials (precatch, normal visual feedback).

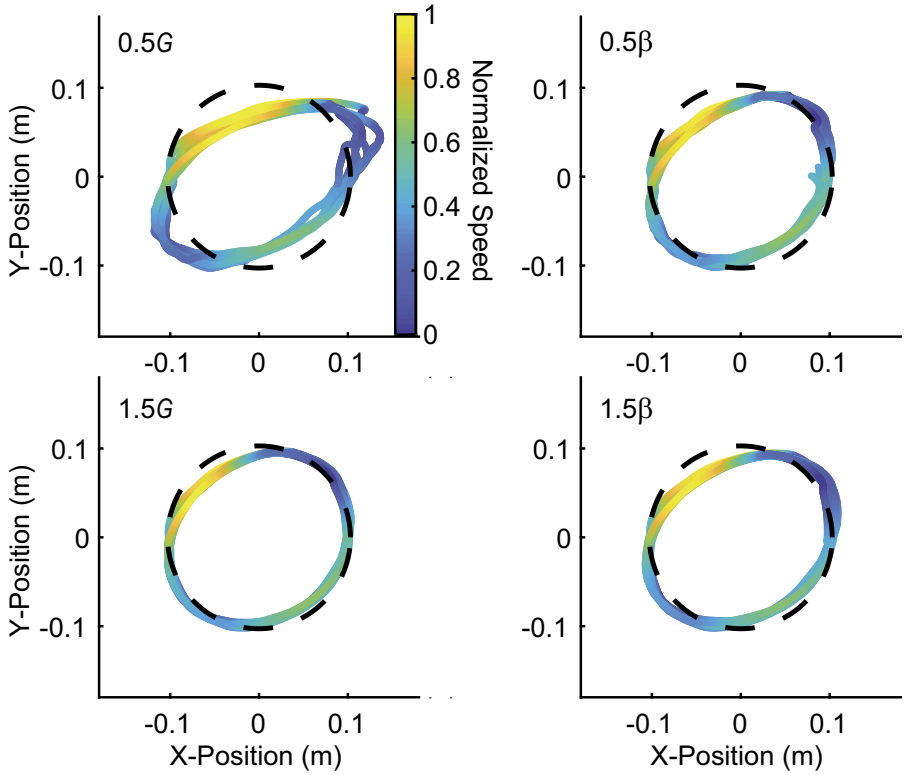

Fig. C1. Representative zero-force trajectories when the impedance parameters were varied over a 3:1 range. G is the gain term for the stiffness and damping (*left*); β is the ratio of stiffness to damping (*right*). These results are from the same example subject and trial presented in Fig. 7. The plots are from the medium speed clockwise direction trials. The path defined by the constraint is shown by the black dashed circle. The zero-force trajectories are shown with lines of variable color. The color bar indicates speed along the zero-force path normalized by its range.

normal unit vector, $\boldsymbol{n}$, and tangential unit vector, $\boldsymbol{e}$. The joint torque is denoted $\boldsymbol{\tau} = [\tau_1,\tau_2]^T$.

From the sum of moments acting on the crank,

$$I\ddot{\theta} + b_c\dot{\theta} = r\boldsymbol{e}^T\boldsymbol{F} \tag{A2}$$

summation of moments about the shoulder,

$$\boldsymbol{M}\ddot{\boldsymbol{q}} + \boldsymbol{h} = \boldsymbol{\tau} - \boldsymbol{J}^T\boldsymbol{F} \tag{A3}$$

and the kinematic relation that equates the acceleration at the handle to the acceleration at the hand,

$$\ddot{\boldsymbol{x}} = \boldsymbol{J}\ddot{\boldsymbol{q}} + \dot{\boldsymbol{J}}\dot{\boldsymbol{q}} = r\left(\ddot{\theta}\boldsymbol{e} - \dot{\theta}^2\boldsymbol{n}\right) \tag{A4}$$

a model of the system can be constructed. Parameters comprising these equations include the mass matrix,

$$\boldsymbol{M}(\boldsymbol{q}) = \begin{bmatrix} m_1 l_{c_1}^2 + m_2\left(l_1^2 + c_2^2 + 2l_1c_2C_2 + I_1 + I_2\right) & m_2\left(c_2^2 + l_1c_2C_2\right) + I_2 \\ m_2\left(c_2^2 + l_1c_2C_2\right) + I_2 & m_2c_2^2 + I_2 \end{bmatrix} \tag{A5}$$

the centrifugal and Coriolis forces,

$$\boldsymbol{h} = \begin{bmatrix} -m_2l_1c_2S_2\left(2\dot{q}_1\dot{q}_2 + \dot{q}_2^2\right) \\ m_2l_1c_2S_2\dot{q}_1^2 \end{bmatrix} \tag{A6}$$

and the Jacobian relating unconstrained differential arm motions to hand motions.

$$\boldsymbol{J} = \begin{bmatrix} -\left(l_1S_1 + l_2S_{12}\right) & -l_2S_{12} \\ l_1C_1 + l_2C_{12} & l_2C_{12} \end{bmatrix} \tag{A7}$$

From *Eqs. A2*, *A3*, and *A4*, the relation in *Eq. A8* can be shown

$$R\ddot{\theta} + H = r\boldsymbol{e}^T\boldsymbol{J}^{-T}\boldsymbol{\tau} \tag{A8}$$

where the configuration-dependent damping is

$$R = I + r^2\boldsymbol{e}^T\boldsymbol{J}^{-T}\boldsymbol{M}\boldsymbol{J}^{-1}\boldsymbol{e} \tag{A9}$$

and the configuration-dependent inertia is

$$H = b_c\dot{\theta} + r\boldsymbol{e}^T\boldsymbol{J}^{-T}\left[\boldsymbol{h} - \boldsymbol{M}\boldsymbol{J}^{-1}\left(r\dot{\theta}^2\boldsymbol{n} + \dot{\boldsymbol{J}}\dot{\boldsymbol{q}}\right)\right] \tag{A10}$$

From *Eqs. A2*, *A3*, and *A4*, we can also solve for **F**,

$$\boldsymbol{F} = \left(\boldsymbol{J}\boldsymbol{M}^{-1}\boldsymbol{J}^T + r^2I^{-1}\boldsymbol{e}\boldsymbol{e}^T\right)^{-1}\left[\boldsymbol{J}\boldsymbol{M}^{-1}\left(\boldsymbol{\tau} - \boldsymbol{h}\right) + \dot{\boldsymbol{J}}\dot{\boldsymbol{q}} + r\dot{\theta}\left(\dot{\theta}\boldsymbol{n} + b_cI^{-1}\boldsymbol{e}\right)\right] \tag{A11}$$

APPENDIX B: TRIALS AT PREFERRED SPEED WITHOUT FEEDBACK

To test whether visual feedback altered behavior, we compared the dependent measures for the catch trial (without visual feedback) and the immediately preceding trial with visual feedback. Figure B1 shows that, even though some of the effects became statistically significant, their magnitude was negligible.

APPENDIX C: VARIED IMPEDANCE

The zero-force trajectory is a construct derived from experimental observations based on several assumptions combined with parameter values from the published literature. To assess the sensitivity of this construct to the assumptions used to compute it, key parameters of the model were varied over a 3:1 range. We expected the zero-force path to change, and it did (Fig. C1). However, the temporal coincidence between curvature and speed extrema was robust.

GRANTS

James Hermus was supported in part by a Harrington Fellowship. Dagmar Sternad was supported by National Institutes of Health Grants R01-HD-087089, R01-HD-081346, NSF-NRI 1637854, NSF-CRCNS 1723998, and NSF-M3X 1825942. Neville Hogan was supported in part by the Eric P. and Evelyn E. Newman Fund, Grants NSF-NRI 1637824, NSF-CRCNS 1724135, NSF-M3X 1826097, and NIH R01-HD-087089.

DISCLOSURES

No conflicts of interest, financial or otherwise, are declared by the authors.

AUTHOR CONTRIBUTIONS

J.D. and N.H. conceived and designed research; J.D. and N.H. performed experiments; J.H. analyzed data; J.H., J.D., D.S., and N.H. interpreted results of experiments; J.H. prepared figures; J.H. drafted manuscript; J.H., J.D., D.S., and N.H. edited and revised manuscript; J.H., J.D., D.S., and N.H. approved final version of manuscript.

REFERENCES

Abend W, Bizzi E, Morasso P. Human arm trajectory formation. *Brain* 105: 331–348, 1982. doi:10.1093/brain/105.2.331.

Bazzi S, Ebert J, Hogan N, Sternad D. Stability and predictability in human control of complex objects. *Chaos* 28: 103103, 2018. doi:10.1063/1.5042090.

Bennett DJ, Hollerbach JM, Xu Y, Hunter IW. Time-varying stiffness of human elbow joint during cyclic voluntary movement. *Exp Brain Res* 88: 433–442, 1992. doi:10.1007/BF02259118.

Bizzi E, Accornero N, Chapple W, Hogan N. Arm trajectory formation in monkeys. *Exp Brain Res* 46: 139–143, 1982. doi:10.1007/BF00238107.

Bizzi E, Accornero N, Chapple W, Hogan N. Posture control and trajectory formation during arm movement. *J Neurosci* 4: 2738–2744, 1984. doi:10.1523/JNEUROSCI.04-11-02738.1984.

Boesch C, Boesch H. Tool use and tool making in wild chimpanzees. *Folia Primatol (Basel)* 54: 86–99, 1990. doi:10.1159/000156428.

Catavitello G, Ivanenko YP, Lacquaniti F, Viviani P. Drawing ellipses in water: evidence for dynamic constraints in the relation between velocity and path curvature. *Exp Brain Res* 234: 1649–1657, 2016. doi:10.1007/s00221-016-4569-9.

Chib VS, Krutky MA, Lynch KM, Mussa-Ivaldi FA. The separate neural control of hand movements and contact forces. *J Neurosci* 29: 3939–3947, 2009. doi:10.1523/JNEUROSCI.5856-08.2009.

Colgate E, Hogan N. An analysis of contact instability in terms of passive physical equivalents. In: *Proceedings, 1989 IEEE International Conference on Robotics and Automation.* Piscataway, NJ: IEEE, 1989, p. 404–409. doi:10.1109/ROBOT.1989.100021.

Colgate JE, Hogan N. Robust control of dynamically interacting systems. *Int J Control* 48: 65–88, 1988. doi:10.1080/00207178808906161.

Dayan E, Casile A, Levit-Binnun N, Giese MA, Hendler T, Flash T. Neural representations of kinematic laws of motion: evidence for action-perception coupling. *Proc Natl Acad Sci USA* 104: 20582–20587, 2007. doi:10.1073/pnas.0710033104.

de Rugy A, Sternad D. Interaction between discrete and rhythmic movements: reaction time and phase of discrete movement initiation during oscillatory movements. *Brain Res* 994: 160–174, 2003. doi:10.1016/j.brainres.2003.09.031.

Doeringer JA. *An Investigation into the Discrete Nature of Human Arm Movements*. Cambridge, MA: Massachusetts Institute of Technology, 1999.

Dohrmann CR, Busby HR, Trujillo DM. Smoothing noisy data using dynamic programming and generalized cross-validation. *J Biomech Eng* 110: 37–41, 1988. doi:10.1115/1.3108403.

Feldman AG. Functional tuning of the nervous system during control of movement or maintenance of a steady posture. II. Controllable parameters of the muscles. *Biophysics (Oxf)* 11: 565–578, 1966.

Feldman AG. Once more on the equilibrium-point hypothesis (lambda model) for motor control. *J Mot Behav* 18: 17–54, 1986. doi:10.1080/00222895.1986.10735369.

Flash T. The control of hand equilibrium trajectories in multi-joint arm movements. *Biol Cybern* 57: 257–274, 1987. doi:10.1007/BF00338819.

Flash T, Hogan N. The coordination of arm movements: an experimentally confirmed mathematical model. *J Neurosci* 5: 1688–1703, 1985. doi:10.1523/JNEUROSCI.05-07-01688.1985.

Fritsch FN, Carlson RE. Monotone piecewise cubic interpolation. *SIAM J Numer Anal* 17: 238–246, 1980. doi:10.1137/0717021.

Georgopoulos AP, Schwartz AB, Kettner RE. Neuronal population coding of movement direction. *Science* 233: 1416–1419, 1986. doi:10.1126/science.3749885.

Gomi H, Kawato M. Equilibrium-point control hypothesis examined by measured arm stiffness during multijoint movement. *Science* 272: 117–120, 1996. doi:10.1126/science.272.5258.117.

Gribble PL, Ostry DJ. Origins of the power law relation between movement velocity and curvature: modeling the effects of muscle mechanics and limb dynamics. *J Neurophysiol* 76: 2853–2860, 1996. doi:10.1152/jn.1996.76.5.2853.

Gribble PL, Ostry DJ, Sanguineti V, Laboissière R. Are complex control signals required for human arm movement? *J Neurophysiol* 79: 1409–1424, 1998. doi:10.1152/jn.1998.79.3.1409.

Guarín DL, Kearney RE. Estimation of time-varying, intrinsic and reflex dynamic joint stiffness during movement. Application to the ankle joint. *Front Comput Neurosci* 11: 51, 2017. doi:10.3389/fncom.2017.00051.

Hicheur H, Vieilledent S, Richardson MJE, Flash T, Berthoz A. Velocity and curvature in human locomotion along complex curved paths: a comparison with hand movements. *Exp Brain Res* 162: 145–154, 2005. doi:10.1007/s00221-004-2122-8.

Hill AV. The heat of shortening and the dynamic constants of muscle. *Proc R Soc London Ser B Biol Sci* 126: 136–195, 1938. doi:10.1098/rspb.1938.0050.

Hogan N. Control and coordination of voluntary arm movements. In: *Proceedings of the 1982 American Control Conference*. Piscataway, NJ: IEEE, 1982, p. 522–528. doi:10.23919/ACC.1982.4787906.

Hogan N. An organizing principle for a class of voluntary movements. *J Neurosci* 4: 2745–2754, 1984. doi:10.1523/JNEUROSCI.04-11-02745.1984.

Hogan N. Impedance control: an approach to manipulation: part I—theory. *J Dyn Syst Meas Control* 107: 1–7, 1985a. doi:10.1115/1.3140702.

Hogan N. Impedance control: an approach to manipulation: part II—implementation. *J Dyn Syst Meas Control* 107: 8–16, 1985b. doi:10.1115/1.3140713.

Hogan N. Physical interaction via dynamic primitives. In: *Geometric and Numerical Foundations of Movements. Springer Tracts in Advanced Robotics*, edited by Laumond J-P, Mansard N, Lasserre J-B. Cham, Switzerland: Springer International, 2017, vol. 117, p. 269–299. doi:10.1007/978-3-319-51547-2_12.

Hogan N, Sternad D. Dynamic primitives of motor behavior. *Biol Cybern* 106: 727–739, 2012. doi:10.1007/s00422-012-0527-1.

Hogan N, Sternad D. Dynamic primitives in the control of locomotion. *Front Comput Neurosci* 7: 71, 2013. doi:10.3389/fncom.2013.00071.

Huh D, Sejnowski TJ. Spectrum of power laws for curved hand movements. *Proc Natl Acad Sci USA* 112: E3950–E3958, 2015. doi:10.1073/pnas.1510208112.

Hunt GR. Manufacture and use of hook-tools by New Caledonian crows. *Nature* 379: 249–251, 1996. doi:10.1038/379249a0.

Johnson-Frey SH. The neural bases of complex tool use in humans. *Trends Cogn Sci* 8: 71–78, 2004. doi:10.1016/j.tics.2003.12.002.

Joyce GC, Rack PMH, Westbury DR. The mechanical properties of cat soleus muscle during controlled lengthening and shortening movements. *J Physiol* 204: 461–474, 1969. doi:10.1113/jphysiol.1969.sp008924.

Kandel E, Schwartz J, Jessell T, Siegelbaum S, Heudspeth AJ (Editors). *Principles of Neural Science* (5th ed.). New York: McGraw-Hill Education, 2013.

Kenward B, Weir AAS, Rutz C, Kacelnik A. Behavioural ecology: tool manufacture by naive juvenile crows. *Nature* 433: 121, 2005. doi:10.1038/433121a.

Khatib O. A unified approach for motion and force control of robot manipulators: the operational space formulation. *IEEE J Robot Autom* 3: 43–53, 1987. doi:10.1109/JRA.1987.1087068.

Kluzik J, Diedrichsen J, Shadmehr R, Bastian AJ. Reach adaptation: what determines whether we learn an internal model of the tool or adapt the model of our arm? *J Neurophysiol* 100: 1455–1464, 2008. doi:10.1152/jn.90334.2008.

Koeppen R, Huber M, Sternad D, Hogan V. Controlling physical interactions: humans do not minimize muscle effort. In: *Proceedings of the ASME 2017 Dynamic Systems and Control Conference*. New York: ASME, 2017, vol. 1, p. V001T36A003. doi:10.1115/DSCC2017-5202.

Krakauer JW, Ghazanfar AA, Gomez-Marin A, MacIver MA, Poeppel D. Neuroscience needs behavior: correcting a reductionist bias. *Neuron* 93: 480–490, 2017. doi:10.1016/j.neuron.2016.12.041.

Lackner JR, Dizio P. Rapid adaptation to Coriolis force perturbations of arm trajectory. *J Neurophysiol* 72: 299–313, 1994. doi:10.1152/jn.1994.72.1.299.

Lacquaniti F, Carrozzo M, Borghese NA. Time-varying mechanical behavior of multijointed arm in man. *J Neurophysiol* 69: 1443–1464, 1993. doi:10.1152/jn.1993.69.5.1443.

Lacquaniti F, Terzuolo C, Viviani P. The law relating the kinematic and figural aspects of drawing movements. *Acta Psychol (Amst)* 54: 115–130, 1983. doi:10.1016/0001-6918(83)90027-6.

Lee H, Ho P, Rastgaar M, Krebs HI, Hogan N. Multivariable static ankle mechanical impedance with active muscles. *IEEE Trans Neural Syst Rehabil Eng* 22: 44–52, 2014a. doi:10.1109/TNSRE.2013.2262689.

Lee H, Hogan N. Time-varying ankle mechanical impedance during human locomotion. *IEEE Trans Neural Syst Rehabil Eng* 23: 755–764, 2015. doi:10.1109/TNSRE.2014.2346927.

Lee H, Krebs HI, Hogan N. Multivariable dynamic ankle mechanical impedance with active muscles. *IEEE Trans Neural Syst Rehabil Eng* 22: 971–981, 2014b. doi:10.1109/TNSRE.2014.2328235.

Lee H, Rouse EJ, Krebs HI. Summary of human ankle mechanical impedance during walking. *IEEE J Transl Eng Health Med* 4: 2100407, 2016. doi:10.1109/JTEHM.2016.2601613.

Loram ID, Maganaris CN, Lakie M. Human postural sway results from frequent, ballistic bias impulses by soleus and gastrocnemius. *J Physiol* 564: 295–311, 2005. doi:10.1113/jphysiol.2004.076307.

Mason MT. Compliance and force control for computer controlled manipulators. *IEEE Trans Syst Man Cybern* 11: 418–432, 1981. doi:10.1109/TSMC.1981.4308708.

Massey JT, Lurito JT, Pellizzer G, Georgopoulos AP. Three-dimensional drawings in isometric conditions: relation between geometry and kinematics. *Exp Brain Res* 88: 685–690, 1992. doi:10.1007/BF00228198.

Maurice P, Hogan N, Sternad D. Predictability, force, and (anti)resonance in complex object control. *J Neurophysiol* 120: 765–780, 2018a. doi:10.1152/jn.00918.2017.

Maurice P, Huber ME, Hogan N, Sternad D. Velocity-curvature patterns limit human-robot physical interaction. *IEEE Robot Autom Lett* 3: 249–256, 2018b. doi:10.1109/LRA.2017.2737048.

Miller DI, Nelson RC. *Biomechanics of Sport: A Research Approach*. Philadelphia, PA: Lee and Febiger, 1973.

Mussa-Ivaldi FA, Hogan N, Bizzi E. Neural, mechanical, and geometric factors subserving arm posture in humans. *J Neurosci* 5: 2732–2743, 1985. doi:10.1523/JNEUROSCI.05-10-02732.1985.

Nasseroleslami B, Hasson CJ, Sternad D. Rhythmic manipulation of objects with complex dynamics: predictability over chaos. *PLOS Comput Biol* 10: e1003900, 2014. doi:10.1371/journal.pcbi.1003900.

Nelson WL. Physical principles for economies of skilled movements. *Biol Cybern* 46: 135–147, 1983. doi:10.1007/BF00339982.

Ohta K, Svinin MM, Luo Z, Hosoe S, Laboissière R. Optimal trajectory formation of constrained human arm reaching movements. *Biol Cybern* 91: 23–36, 2004. doi:10.1007/s00422-004-0491-5.

Paul R. Problems and research issues associated with the hybrid control of force and displacement. In: *Proceedings. 1987 IEEE International Conference on Robotics and Automation*. Piscataway, NJ: IEEE, 1987, p. 1966–1971. doi:10.1109/ROBOT.1987.1087905.

Plagenhoef S. *Patterns of Human Motion: A Cinematographic Analysis*. Englewood Cliffs, NY: Prentice-Hall, 1971.

Rack PMH, Westbury DR. The effects of length and stimulus rate on tension in the isometric cat soleus muscle. *J Physiol* 204: 443–460, 1969. doi:10.1113/jphysiol.1969.sp008923.

Raibert MH, Craig JJ. Hybrid position/force control of manipulators. *J Dyn Syst Meas Control* 103: 126–133, 1981. doi:10.1115/1.3139652.

Rancourt D, Hogan N. Stability in force-production tasks. *J Mot Behav* 33: 193–204, 2001. doi:10.1080/00222890109603150.

Rancourt D, Hogan N. The biomechanics of force production. In: *Progress in Motor Control. Advances in Experimental Medicine and Biology*, edited by Sternad D. Boston, MA: Springer, 2009, vol. 629, p. 645–661. doi:10.1007/978-0-387-77064-2_35.

Richardson MJE, Flash T. Comparing smooth arm movements with the two-thirds power law and the related segmented-control hypothesis. *J Neurosci* 22: 8201–8211, 2002. doi:10.1523/JNEUROSCI.22-18-08201.2002.

Ronsse R, Sternad D, Lefèvre P. A computational model for rhythmic and discrete movements in uni- and bimanual coordination. *Neural Comput* 21: 1335–1370, 2009. doi:10.1162/neco.2008.03-08-720.

Rouse EJ, Hargrove LJ, Perreault EJ, Kuiken TA. Estimation of human ankle impedance during the stance phase of walking. *IEEE Trans Neural Syst Rehabil Eng* 22: 870–878, 2014. doi:10.1109/TNSRE.2014.2307256.

Rouse EJ, Hargrove LJ, Perreault EJ, Peshkin MA, Kuiken TA. Development of a mechatronic platform and validation of methods for estimating ankle stiffness during the stance phase of walking. *J Biomech Eng* 135: 81009, 2013. doi:10.1115/1.4024286.

Russell D, Hogan N. Dealing with constraints: a biomechanical approach. In: *Images of the Twenty-First Century. Proceedings of the Annual International Engineering in Medicine and Biology Society*. Piscataway, NJ: IEEE, 1989, vol. 3, p. 892–893. doi:10.1109/IEMBS.1989.96034.

Schaal S, Sternad D. Programmable pattern generators. *3rd International Conference on Computational Intelligence in Neuroscience*, Research Triangle Park, NC, 1998, p. 48–51.

Schaal S, Sternad D. Origins and violations of the 2/3 power law in rhythmic three-dimensional arm movements. *Exp Brain Res* 136: 60–72, 2001. doi:10.1007/s002210000505.

Schwartz AB. Direct cortical representation of drawing. *Science* 265: 540–542, 1994. doi:10.1126/science.8036499.

Shampine LF, Reichelt MW. The MATLAB ODE suite. *SIAM J Sci Comput* 18: 1–22, 1997. doi:10.1137/S1064827594276424.

Shepard RN, Metzler J. Mental rotation of three-dimensional objects. *Science* 171: 701–703, 1971. doi:10.1126/science.171.3972.701.

Slotine J-JE, Asada H. *Robot Analysis and Control*. New York: Wiley, 1992.

Sternad D. Towards a unified theory of rhythmic and discrete movements—behavioral, modeling and imaging results. In: *Coordination: Neural, Behavioral and Social Dynamics. Understanding Complex Systems*, edited by Fuchs A and Jirsa VK. Berlin: Springer, 2008, p. 105–133.

Sternad D. Human control of interactions with objects—variability, stability and predictability. In: *Geometric and Numerical Foundations of Movements. Springer Tracts in Advanced Robotics*, edited by Laumond JP, Mansard N, Lasserre JB. Cham, Switzerland: Springer, 2017, vol. 117, p. 301–335.

Sternad D, Dean WJ, Schaal S. Interaction of rhythmic and discrete pattern generators in single-joint movements. *Hum Mov Sci* 19: 627–664, 2000. doi:10.1016/S0167-9457(00)00028-2.

Sternad D, Hasson CJ. Predictability and robustness in the manipulation of dynamically complex objects. In: *Progress in Motor Control. Advances in Experimental Medicine and Biology*, edited by Laczko J, Latash M. Cham, Switzerland: Springer, 2016, vol. 957, p. 55–77.

Sternad D, Park S-W, Müller H, Hogan N. Coordinate dependence of variability analysis. *PLOS Comput Biol* 6: e1000751, 2010. doi:10.1371/journal.pcbi.1000751.

Sternad D, Schaal S. Segmentation of endpoint trajectories does not imply segmented control. *Exp Brain Res* 124: 118–136, 1999. doi:10.1007/s002210050606.

van de Ruit M, Cavallo G, Lataire J, van der Helm FCT, Mugge W, van Wingerden J-W, Schouten AC. Revealing time-varying joint impedance with kernel-based regression and nonparametric decomposition. In: *IEEE Transactions on Control Systems Technology*. Piscataway, NJ: IEEE, 2020, vol. 28, no. 1,p. 224–237. doi:10.1109/TCST.2018.2881664.

Viviani P, Flash T. Minimum-jerk, two-thirds power law, and isochrony: converging approaches to movement planning. *J Exp Psychol Hum Percept Perform* 21: 32–53, 1995. doi:10.1037/0096-1523.21.1.32.

Viviani P, Stucchi N. The effect of movement velocity on form perception: geometric illusions in dynamic displays. *Percept Psychophys* 46: 266–274, 1989. doi:10.3758/BF03208089.

Viviani P, Terzuolo C. Trajectory determines movement dynamics. *Neuroscience* 7: 431–437, 1982. doi:10.1016/0306-4522(82)90277-9.

Whitney DE. Force feedback control of manipulator fine motions. *J Dyn Syst Meas Control* 99: 91–97, 1977. doi:10.1115/1.3427095.

Wolpert DM, Ghahramani Z, Jordan MI. Are arm trajectories planned in kinematic or dynamic coordinates? An adaptation study. *Exp Brain Res* 103: 460–470, 1995. doi:10.1007/BF00241505.

Wolpert DM, Miall RC, Kawato M. Internal models in the cerebellum. *Trends Cogn Sci* 2: 338–347, 1998. doi:10.1016/S1364-6613(98)01221-2.

Won J, Hogan N. Stability properties of human reaching movements. *Exp Brain Res* 107: 125–136, 1995. doi:10.1007/BF00228024.

Zago M, Matic A, Flash T, Gomez-Marin A, Lacquaniti F. The speed-curvature power law of movements: a reappraisal. *Exp Brain Res* 236: 69–82, 2018. doi:10.1007/s00221-017-5108-z.